A&A 635, A74 (2020)
https://doi.org/10.1051/0004-6361/201937334

Astronomy & Astrophysics

A multiplicity study of transiting exoplanet host stars

II. Revised properties of transiting planetary systems with companions⋆

J. Southworth[1], A. J. Bohn[2], M. A. Kenworthy[2], C. Ginski[3], and L. Mancini[4,5,6,7]

[1] Astrophysics Group, Keele University, Staffordshire ST5 5BG, UK
e-mail: astro.js@keele.ac.uk
[2] Leiden Observatory, Leiden University, PO Box 9513, 2300 RA Leiden, The Netherlands
[3] Sterrenkundig Instituut Anton Pannekoek, Science Park 904, 1098 XH Amsterdam, The Netherlands
[4] Department of Physics, University of Rome Tor Vergata, Via della Ricerca Scientifica 1, 00133 Rome, Italy
[5] Max Planck Institute for Astronomy, Königstuhl 17, 69117 Heidelberg, Germany
[6] INAF – Osservatorio Astrofisico di Torino, via Osservatorio 20, 10025 Pino Torinese, Italy
[7] International Institute for Advanced Scientific Studies (IIASS), Via G. Pellegrino 19, 84019 Vietri sul Mare (SA), Italy

Received 17 December 2019 / Accepted 21 January 2020

ABSTRACT

Context. Binarity is a widespread phenomenon around solar-type stars, including the host stars of transiting extrasolar planets.
Aims. We performed a detailed study of six transiting planetary systems with relatively bright stars close enough to affect observations of these systems. These contaminants were characterised in a companion work.
Methods. We used theoretical spectra to propagate the observed K-band light ratios into the optical passbands used to observe these systems. Light curves were analysed whilst taking the contaminating light and its uncertainty into account. We present and applied a method to correct the velocity amplitudes of the host stars for the presence of contaminating light.
Results. We determined the physical properties of six systems (WASP-20, WASP-70, WASP-8, WASP-76, WASP-2, and WASP-131) whilst accounting for contaminating light. In the case of WASP-20, the measured physical properties are very different for the three scenarios considered: ignoring binarity, planet transits brighter star, and planet transits fainter star. In the other five cases, our results are very similar to those obtained when neglecting contaminating light. We used our results to determine the mean correction factors to planet radius, $\langle X_{\rm R}\rangle$, mass, $\langle X_{\rm M}\rangle$, and density, $\langle X_\rho\rangle$, caused by nearby objects. We find $\langle X_{\rm R}\rangle = 1.009 \pm 0.045$, which is smaller than literature values because we were able to reject the possibility that the planet orbits the fainter star in all but one case. We find $\langle X_{\rm M}\rangle = 1.031 \pm 0.019$, which is larger than $\langle X_{\rm R}\rangle$ because of the strength of the effect of contaminating light on the radial velocity measurements of the host star. We find $\langle X_\rho\rangle = 0.995 \pm 0.046$: the small size of this correction is due to two effects: the corrections on planet radius and mass partially cancel; and some nearby stars are close enough to contaminate the light curves of the system but not radial velocities of the host star. These corrections can be applied to samples of transiting hot Jupiters to statistically remove biases due to light contamination.
Conclusions. We conclude that binarity of planet host stars is important for the small number of transiting hot Jupiters with a very bright and close nearby star, but it has only a small effect on population-level studies of these objects.

Key words. planetary systems – stars: fundamental parameters – techniques: high angular resolution – binaries: visual

1. Introduction

The detection and characterisation of extrasolar planets is widespread and rapidly evolving. The vast majority of the early detections were via the radial velocity (RV) method, in which the orbital motion of the host star is observed (Mayor & Queloz 1995; Marcy & Butler 1996; Udry & Santos 2007). This technique yields measurements of the orbital period, eccentricity, and separation, plus a lower limit on the mass of the planet. The dominant detection technique is currently the transit method, in which the drop in brightness of the host star due to the transit of the planet is observed. The transit method is useful for only a small fraction of planets, as the vast majority do not transit their host star, but it is highly efficient because thousands of stars can be surveyed simultaneously (e.g. Bakos et al. 2002; Pollacco et al. 2006; Borucki et al. 2010). When combined for a single system, the RV and transit methods allow the full physical properties of the planetary system to be calculated: mass, radius, density, and surface gravity of both star and planet.

One of the basic assumptions of the transit method is that the light from the host star is not contaminated by light from a nearby star. If this assumption is incorrect, the measured physical properties of the system are biased away from their true values. The contamination causes a bias in two ways. Firstly, the contaminating light dilutes the light from the host star, thus decreasing the depth of the transit and leading to an underestimate of the radius of the transiting planet (e.g. Daemgen et al. 2009; Southworth 2010). Secondly, spectral lines from the nearby star blend with those from the planet host star, which potentially cause the orbital motion of the star (and thus the mass of the planet) to be underestimated (Buchhave et al. 2011; Evans et al. 2016a). If ignored, contaminating light systematically affects the properties measured for populations of planets and their host stars, rendering unsafe any conclusions on the formation and evolution of planetary systems based on these demographics.

⋆ Based on observations collected at the European Organisation for Astronomical Research in the Southern Hemisphere under ESO programmes 098.C-0589(A) and 099.C-0155(A).

Our previous work on WASP-20 (Evans et al. 2016a) showed both effects very clearly, demonstrating the importance of correcting for contamination when determining the physical properties of a transiting planetary system. Using high-resolution adaptive-optics imaging, Evans et al. showed that the WASP-20 system is composed of a resolved binary star, with a separation of 0.2578 ± 0.0007 arcsec, one of which is the host of a transiting planet (Anderson et al. 2015). Analysis of the available data yielded a mass and radius of the planet of 0.291 ± 0.017 $M_{\rm Jup}$ and 1.20 ± 0.14 $R_{\rm Jup}$ ignoring binarity, 0.378 ± 0.022 $M_{\rm Jup}$ and 1.28 ± 0.15 $R_{\rm Jup}$ if the planet orbits the brighter star, and 1.30 ± 0.19 $M_{\rm Jup}$ and 1.69 ± 0.12 $R_{\rm Jup}$ if the planet orbits the fainter star. This shows that binarity and light contamination can have a large effect on the measured properties of the planet.

Buchhave et al. (2011) found comparable results for the planetary system Kepler-14, one component of a visual binary with a separation of 0.28″ and a magnitude difference of $\Delta V = 0.52 \pm 0.05$ mag. These authors found that correcting for the presence of the nearby star increased the mass and radius of the planet by 60 and 10%, respectively. Buchhave et al. (2011) were able to show that the planet orbits the brighter of the two stars by analysing the motion of the flux-weighted centroid of the binary during transit.

Another problem caused by contaminating light is the modification of the transmission spectrum of a transiting planet. A transmission spectrum is obtained by measuring the transit depth as a function of wavelength (Seager & Sasselov 2000; Brown 2001). Unless the contaminating star has the same spectral energy distribution as the planet host star, its light could imprint a wavelength-dependent signal on the transit depth that could be erroneously interpreted as arising from the atmosphere of the planet. As an example, Southworth et al. (2015) found a strong Rayleigh scattering slope in the atmosphere of the planet WASP-103 b. A faint nearby star was subsequently detected by Wöllert & Brandner (2015), and a reanalysis of the transit data by Southworth & Evans (2016) yielded a significant modification to the transmission spectrum of the planet

Aside from the implications on measurements of the properties of planetary systems, the multiplicity of planet host stars is intrinsically interesting. Hot Jupiters cannot form in such tight orbits due to the high temperature and lack of mass available in this part of the protoplanetary disc (Boss 1995; Lin et al. 1996) so must form further out and migrate inwards (see Baruteau et al. 2014; Davies et al. 2014). Smooth migration by interactions with the disc (Lin et al. 1996) cannot explain the existence of hot Jupiters on eccentric or misaligned orbits (Wu & Murray 2003; Fabrycky & Tremaine 2007). This suggests that gravitational interactions with a third body must be involved in the migration of at least a subset of hot Jupiters, either through planet–planet scattering events (Rasio & Ford 1996; Chatterjee et al. 2008) or the Kozai–Lidov mechanism (Fabrycky & Tremaine 2007; Naoz et al. 2011). These predictions can be tested by assessing the fraction of planet host stars that are members of binary or higher-order multiple systems (Knutson et al. 2014).

Third bodies may also inhibit planet formation (Fragner et al. 2011; Roell et al. 2012; Wang et al. 2015). Kraus et al. (2016) found a paucity of binary companions to transiting planetary systems detected using the *Kepler* satellite, compared to expectations from the binarity of field stars. Ziegler et al. (2020) obtained high-resolution imaging of 524 planet candidates discovered using the Transiting Exoplanet Survey Satellite (TESS; Ricker et al. 2015) and found that the fraction of close companions was lower for projected separations <100 au and higher for larger separations, to significance levels of 9.1σ and 4.9σ, respectively. Similar trends were also found by Ngo et al. (2016) for 77 hot Jupiter systems. This implies that closer companions inhibit planet formation but that wider companions either aid planet formation and/or help the inward migration of planets to the relatively short orbital periods where they have been detected (but see also Moe & Kratter 2019).

In a companion paper (Bohn et al. 2020, hereafter Paper I) we presented high-resolution imaging observations of 45 transiting planet host stars, obtained using the SPHERE extreme adaptive-optics instrument on the Very Large Telescope (VLT) (Beuzit et al. 2019). We detected close companions in 26 systems, of which half were previously unknown. Our K-band contrast values were on average 7.0 mag at 0.2″ and 8.9 mag at separations beyond 1″, allowing us to probe for companions down to the hydrogen-burning limit in the majority of our targets. The resulting multiplicity fraction of $55.4^{+5.9}_{-9.4}$% is larger than but in agreement with previous assessments. In the current work we redetermined the physical properties of a subset of the targets from Paper I, accounting for the presence of the nearby companion. In several cases we analysed new photometry from space missions or from our own observations. Section 2 outlines our methods for photometric and spectroscopic observations, Sect. 3 presents our results, Sect. 4 quantifies the impact of contamination on the population of hot Jupiters, and Sect. 5 summarises our work.

2. Methods

2.1. Correcting the light curve for contamination

The amount of contaminating light is a standard parameter in the study of eclipsing binary systems, where it is typically referred to as "third light" (e.g. Kopal 1959). We use the definition that third light, L_3, is the fraction of the total light of the system arising from the third body, neglecting proximity effects in the inner binary system. In order to include this in the model of the transit light curve, it is necessary to determine the amount of contaminating light in the passband used to obtain the light curve. This information is in general not directly measured, but can be determined by using synthetic spectra to extrapolate the flux ratio from the band it was measured in (in our case K) to the band the light curve was obtained in.

We interpolated within the grids of BT-Settl synthetic spectra to obtain spectra for the specific $T_{\rm eff}$ values of the presumed planet host star and the fainter nearby star. These were then scaled to the flux ratio we measured in the K-band, using the transmission profile for the SPHERE K_s filter[1]. Both spectra were then convolved with the profile of the relevant filter (see below for details) in order to determine the flux ratio in the passband used to obtain the transit light curve.

The uncertainties were propagated by repeating this analysis with the K-band magnitude difference perturbed by its upper and lower errorbar, and then applying this process to the $T_{\rm eff}$s of both the planet host and the nearby star. The individual uncertainties were added in quadrature. The relevant quantities are reported in Table 1.

Modelling the light curves. We followed the precepts of the Homogeneous Studies project (see Southworth 2012, and references therein) to model the best available transit light curve for each target. We summarise the process here. The transits were fitted using the JKTEBOP code (see Southworth 2013, and references therein), which parameterises the system using the

[1] https://www.eso.org/sci/facilities/paranal/instruments/sphere/inst/filters.html

Table 1. Summary of the high-resolution imaging results for the targets in this study.

System	Primary star $T_{\rm eff}$ (K)	Separation (arcsec)	ΔK (mag)	Companion mass ($M_\odot$)	Companion $T_{\rm eff}$ (K)
WASP-20	6000 ± 100	0.259 ± 0.003	0.86 ± 0.06	$0.89^{+0.06}_{-0.07}$	5235^{+242}_{-272}
WASP-70	5700 ± 80	3.160 ± 0.004	1.38 ± 0.18	$0.70^{+0.06}_{-0.07}$	4504^{+263}_{-213}
WASP-8	5600 ± 80	4.520 ± 0.005	2.29 ± 0.08	0.53 ± 0.02	3758^{+47}_{-43}
WASP-76	6250 ± 100	0.436 ± 0.003	2.30 ± 0.05	0.78 ± 0.03	4824^{+126}_{-128}
WASP-2	5170 ± 60	0.710 ± 0.003	2.55 ± 0.07	0.40 ± 0.02	3523^{+28}_{-19}
WASP-131	5950 ± 100	0.189 ± 0.003	2.82 ± 0.20	$0.62^{+0.05}_{-0.04}$	4109^{+200}_{-163}

Notes. Quantities are taken from Paper I. The objects are given in order of increasing K-band magnitude difference (ΔK), as this is the order in which they were analysed in the current work.

fractional radii of the planet and its host star ($r_{\rm A} = \frac{R_{\rm A}}{a}$ and $r_{\rm b} = \frac{R_{\rm b}}{a}$ where $R_{\rm A}$ and $R_{\rm b}$ are the true radii of the star and planet and a is the orbital semimajor axis), the orbital inclination (i), the orbital period ($P_{\rm orb}$), and a reference time of mid-transit (T_0). Limb darkening was included using each of five parametric "laws" (see Southworth 2008) and third light was included using the values found in Sect. 2.1.

The fitted parameters in each case were the sum of the fractional radii, $r_{\rm A} + r_{\rm b}$, the ratio of the radii, $k = \frac{r_{\rm b}}{r_{\rm A}}$, i, and T_0. In some cases one limb darkening coefficient was also fitted. Their uncertainties were obtained using both Monte Carlo and residual permutation algorithms, and the larger of the two possibilities was adopted for each parameter. In all cases the uncertainty of the third light value was accounted for. The error estimates were increased to account for the variations between results obtained using the different limb darkening laws.

2.2. Correcting the radial velocities for contamination

The orbital motion of each planet host star has been measured as part of the process of confirming the planetary nature of the transiting companion. This was done by obtaining multiple high-resolution spectra, calculating the cross-correlation function (CCF) of each versus a numerical mask (Baranne et al. 1996), measuring the centroid of each CCF to obtain the RV, and fitting the RVs with a spectroscopic orbit. The amplitude of this orbit was then used in the measurement of the mass of the planet.

If the light from a nearby star contaminates the observed spectrum, it may bias the RVs measured from the CCFs away from the true value, affecting the measured mass of the planet. The size of this effect depends on multiple factors: (1) the light ratio of the contaminant versus the planet host star; (2) the fraction of light from the contaminant that enters the spectrograph slit or fibre; (3) the strength of the response of the spectrum of the contaminant to the numerical mask used to obtain the CCF; (4) the velocity difference between the host star and contaminant; and (5) the projected rotational velocities ($v \sin i$) of the two stars. The effect for point 2 is wavelength-dependent and thus is affected by both the spectral energy distribution of the two stars and the number of spectral lines involved in the RV measurement process as a function of wavelength.

This bias must be corrected for in order to measure the mass of the planet correctly, which means that it must be calculated. We constructed a simple model to estimated the correction factor for a system with a given light ratio, RV separation between the planet host and contaminant, and the $v \sin i$ values of the two stars. We used Gaussian functions to approximate the CCFs, with the expectation that this would induce significantly smaller inaccuracy than the assumptions we were forced to make on the spectral characteristics of the contaminating star (see above). More sophisticated simulations would ideally use true stellar spectra injected into the RV measurement pipeline for every observed spectrum, something outside the scope of the current work.

The correction factor was defined to be the true RV divided by the RV measured from the composite CCF. This definition means that the correction factors are usually above unity, and can become significantly larger than unity when the RV bias is large.

In each case, we used published measurements of the $v \sin i$ of the planet host star. In the absence of measurements of $v \sin i$ for the contaminating star we assumed a representative value of 2 ± 1 km s^{-1}. The RV separation was taken to be the velocity amplitude of the host star's spectroscopic orbit, $K_{\rm A}$, which incurs two assumptions: the bias affecting the RVs away from quadrature scales linearly with RV separation; and the contaminating star is at the systemic velocity and thus is gravitationally bound to the planet host star on a wide orbit. We then generated Gaussian functions for the two CCFs, added them together, and fitted the composite CCF with a single Gaussian to determine the correction factor between the true and the measured RV of the planet host star.

The $v \sin i$ values used in this analysis were assumed to be full widths at half maximum (FWHMs). These were corrected to standard deviations, by dividing by $2\sqrt{2 \ln 2}$, in order to generate the Gaussian functions used for the CCFs.

Uncertainties in the correction factor were assessed by perturbing the input properties by their uncertainties (when known) or by a reasonable amount (when not known, and when possible). Linear interpolation was used in grids of correction factors in order to determine the value and uncertainty of the final number. A set of plots showing the behaviour of the correction factor is given during the discussion of WASP-20 below.

In all cases it must be borne in mind that the correction factor depends on our assumptions, and could even be negligibly different from unity if the RV of the contaminating star differs significantly from the systemic velocity of the planetary system. However, in the latter case, some systems would be picked up as having double-lined spectra indicative of either a contaminating star or an eclipsing binary system, so would be less likely to be ushered through the process of verifying that the transiting body is indeed a planet.

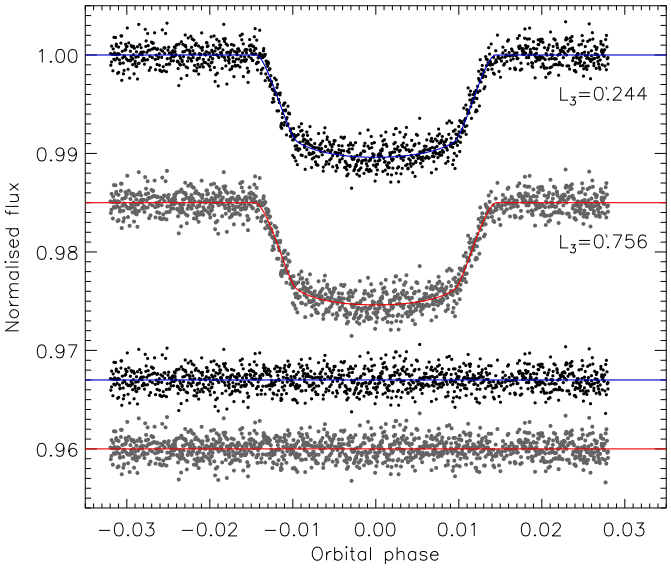

Fig. 1. Fits to the TESS light curve of WASP-20. The observational data are shown as black and grey points. The JKTEBOP best fit for the planet transiting star A is the blue line, and for transiting star B is the red line. The residuals of the fits are shown at the base of the figure with arbitrary offsets from zero.

2.3. Determining the physical properties of the systems

Once measured values of r_A, r_b, i, P_{orb}, and K_A were available, these were combined with tabulated predictions from theoretical evolution models for the properties of the planet host star (Southworth 2009, 2010). The physical properties of the systems were calculated using the velocity amplitude of the planet, K_b, determined by iteratively maximising the agreement between the measured and predicted T_{eff} and r_A for the host star.

The uncertainties on the input parameters were propagated by a perturbation analysis to give statistical errorbars. The variations in results, from the use of five different sets of theoretical model predictions, were used to estimate the systematic errors for the output parameters. Both errorbars are given for all quantities that have a systematic error in their measurement.

3. Results for individual systems

The underestimation of the planet mass and radius is larger for stronger contamination, so in what follows we consider each planetary system in decreasing order of contamination level, until we reach those systems where the biases are negligible. It is important to remember that we cannot simply fit for the contamination level when modelling a transit light curve, as there is insufficient information in the light curve[2] (see Southworth 2010).

3.1. WASP-20

WASP-20 was previously presented as a poster child of the effect of contaminating light on the characterisation of a transiting planetary system (Evans et al. 2016a). The discovery and first analysis of the system (Anderson et al. 2015) proceeded under the assumption that the star was single, but an image from the SPHERE instrument showed it to be a double system separated by 0.26″ and with a magnitude difference of $\Delta K = 0.86$. Evans et al. (2016a) modelled the best transit light curve then available for three scenarios: ignoring binarity; the planet orbits the brighter star; and the planet orbits the fainter star. The available data were insufficient to determine which of the last two scenarios was the correct one, although the planet-orbits-brighter-star was preferred. The measured mass and radius of the planet under these two scenarios differed by factors of 3.4 and 1.3, respectively. Both were also significantly different from the values obtained without accounting for the presence of contaminating light.

We have revisited this system for two reasons: a much better transit light curve is now available from the TESS satellite; and a more precise spectroscopic analysis of the host star has been published (Andreasen et al. 2017). The spectroscopic analysis was performed without accounting for contamination from the secondary star, so the results will be slightly biased; it is beyond the scope of the current work to account for this effect.

3.1.1. Photometric analysis

Andreasen et al. (2017) determined the T_{eff} of the WASP-20 system to be 5987 ± 20 K. We took this to represent the brighter (and presumed planet host) star as it dominates the optical flux of the system. Using the K-band magnitude difference and contaminating star T_{eff} from Table 1, we determined a light ratio in the TESS passband of 0.323 ± 0.063. The contaminating light therefore contributes a fraction of 0.244 ± 0.048 of the light of the system.

The TESS data[3] cover six transits in short cadence and were downloaded from the MAST archive[4]. Each transit was extracted from the full light curve and normalised to unit flux by fitting a straight line to the adjacent out-of-transit data. The resulting data were modelled with the JKTEBOP code as described above and the results are given in Table 2 and shown in Fig. 1.

3.1.2. Correction factor

The star dominating the spectrum was found to have $v \sin i = 4.7 \pm 0.5$ km s^{-1} and a velocity amplitude $K_A = 32.8 \pm 1.7$ m s^{-1} by Anderson et al. (2015). We have assumed that this $v \sin i$ represents the brighter of the two stars: this assumption is questionable but a useful improvement would require effort beyond the scope of the current work. We used the light ratio of 0.323 but inflated the uncertainty for this value to 0.1 for the reasons described in Sect. 2.2. We found a correction factor of 1.34 with errorbars of ±0.02 from the $v \sin i$ of the brighter star, ±0.08 from the $v \sin i$ of the fainter star, and ±0.12 for the light ratio. Adding these uncertainties in quadrature gives a correction factor of 1.34 ± 0.14. This yields a velocity amplitude of 44.0 ± 5.1 m s^{-1}, where the uncertainties from the measurement and from the correction factor have again been added in quadrature.

Evans et al. (2016a) found a correction factor of 1.37 ± 0.05 for WASP-20 (after adjusting for their different definition of this quantity). This is in very good agreement with our value, despite the use of a different (actually more sophisticated) method and the erroneous use of $v \sin i = 2$ km s^{-1} for the brighter star. Our larger errorbar comes from the inclusion of more sources of uncertainty than those considered by Evans et al. (2016a), and it likely a better indicator of the intrinsic uncertainty of the correction factor.

[2] It becomes possible to measure the contamination level when it contributes approximately 90% of the total light or more; see Bognár et al. (2015).

[3] Application: G011112, PI: J. Southworth.

[4] https://mast.stsci.edu/portal/Mashup/Clients/Mast/Portal.html

Table 2. Derived physical properties for the WASP-20 system.

Parameter	Symbol	Anderson et al. (2015)	Planet transits brighter star (adopted solution)	Planet transits fainter star
Sum of the fractional radii	$r_A + r_b$		0.1100 ± 0.0036	$0.0918^{+0.0032}_{-0.0019}$
Ratio of the radii	$k = R_b/R_A$	0.1079 ± 0.0011	0.1143 ± 0.0040	0.192 ± 0.014
Inclination (°)	i	85.56 ± 0.22	86.36 ± 0.33	89.24 ± 0.87
Fractional radius of the star	$r_A = R_A/a$	0.1078 ± 0.0027	0.0987 ± 0.0034	$0.0770^{+0.0035}_{-0.0019}$
Fractional radius of the planet	$r_b = R_b/a$		0.01129 ± 0.00046	0.01481 ± 0.00080
Stellar mass ($M_\odot$)	M_A	1.200 ± 0.041	$1.113 \pm 0.027 \pm 0.021$	0.900 ± 0.088
Stellar radius ($R_\odot$)	R_A	1.392 ± 0.044	$1.242 \pm 0.044 \pm 0.008$	0.903 ± 0.052
Stellar surface gravity (cgs)	$\log g_A$	4.231 ± 0.020	$4.296 \pm 0.030 \pm 0.003$	4.481 ± 0.043
Stellar density ($\rho_\odot$)	ρ_A	0.447 ± 0.033	0.581 ± 0.060	1.22 ± 0.17
Age (Gyr)	τ	7^{+2}_{-1}	$4.3^{+0.8\ +0.9}_{-1.3\ -1.3}$	$3.3^{+17.0\ +3.9}_{-0.2\ \ -2.1}$
Planet mass (M_{Jup})	M_b	0.311 ± 0.017	$0.396 \pm 0.046 \pm 0.005$	0.998 ± 0.087
Planet radius (R_{Jup})	R_b	1.462 ± 0.059	$1.382 \pm 0.057 \pm 0.008$	1.69 ± 0.11
Planet surface gravity (m s^{-2})	g_b	2.530 ± 0.036	5.13 ± 0.73	8.7 ± 1.1
Planet density (ρ_{Jup})	ρ_b	0.099 ± 0.012	$0.140 \pm 0.024 \pm 0.001$	0.193 ± 0.034
Equilibrium temperature (K)	T_{eq}	1379 ± 31	1330 ± 25	1027 ± 52
Orbital semimajor axis (au)	a	0.0600 ± 0.0007	$0.05851 \pm 0.00047 \pm 0.00036$	0.0545 ± 0.0018

Notes. Where two sets of errorbars are given, the first is the statistical uncertainty and the second is the systematic uncertainty.

If we turn to the alternative scenario of the planet orbiting the fainter star, we find a correction factor of 3.9 ± 1.6. The errorbar is the quadrature addition of individual errorbars of ± 1.1 from the $v \sin i$ of the fainter star, ± 0.1 from the $v \sin i$ of the brighter star, and ± 1.1 for the light ratio. Evans et al. (2016a) found 5.56 ± 0.63 for this scenario, which is approximately 1σ from our own value. The debiassed velocity amplitude from our correction factor is 128 ± 7 m s^{-1}.

Figure 2 shows the results of an exploration of the dependence of the correction factor on the properties of the system assumed in its calculation, for the scenario where the brighter star hosts the planet. The top two panels show how it varies with the $v \sin i$ values of the host star and the contaminant. The dependence is relatively weak in the former case. We attribute this to the orbital motion being much smaller than the widths of the CCFs, so the precise positioning of the flux within the composite CCF does not have much effect on its measured centroid. The third panel shows that the correction factor is much more affected by the light ratio, as expected because a stronger dilution will naturally lead to a stronger bias in the measured RVs. The final panel is included for illustration, and shows how the correction factor depends on the RV separation of the system. The vertical dashed line indicates the true velocity amplitude of the planet host star as determined from the measured velocity amplitude and the correction factor found above. For reference, Fig. 3 shows the variation of the correction factor in the case that the planet orbits the fainter of the two stars.

3.1.3. Physical properties

We determined the physical properties of the WASP-20 planetary system under both scenarios: planet orbits brighter star and planet orbit fainter star. Andreasen et al. (2017) determined the T_{eff} of the WASP-20 system to be 5987 ± 20 K, and we used this value in preference to the value of 6000 ± 100 K adopted for Paper I. We inflated the errorbar to 50 K as this is the level of variation between different high-quality analyses of similar stars (e.g. De Pascale et al. 2014; Gómez Maqueo Chew et al. 2014; Ryabchikova et al. 2016). Andreasen et al. (2017) also quoted a metallicity of [Fe/H] $= 0.07 \pm 0.02$; we have adopted this with a larger errorbar of 0.05 dex for similar reasons (see e.g. Jofré et al. 2014; De Pascale et al. 2014).

Physical properties were obtained for the two scenarios, using the method outline in Sect. 2.3. We used the respective T_{eff} values of the two stars and, under the assumption of physical relation, the same metallicity value. Table 2 contains the results and shows that the measured planet properties change significantly between the two scenarios. The mass of the planet is most affected, being $0.40 \pm 0.05\ M_{Jup}$ if the planet orbits the brighter star and $1.00 \pm 0.09\ M_{Jup}$ if it orbits the fainter. This is in good agreement with the results of Evans et al. (2016a). The inclusion of the TESS data in our analysis has allowed the radius of the planet to be measured to a greater precision compared to previous work.

3.2. WASP-70

WASP-70 is the system with the second-brightest nearby companion, with $\Delta K = 1.38 \pm 0.18$ mag and a separation of $3.2''$. The companion was detected in the discovery paper of the system (Anderson et al. 2014) and in subsequent Lucky Imaging (Wöllert & Brandner 2015; Ginski et al. 2016; Evans et al. 2018) and adaptive-optics (Ngo et al. 2016) studies. In Paper I we established that its proper motion is consistent with it being a bound, not background, object. Anderson et al. (2014) accounted for the companion star by removing its contribution from the light

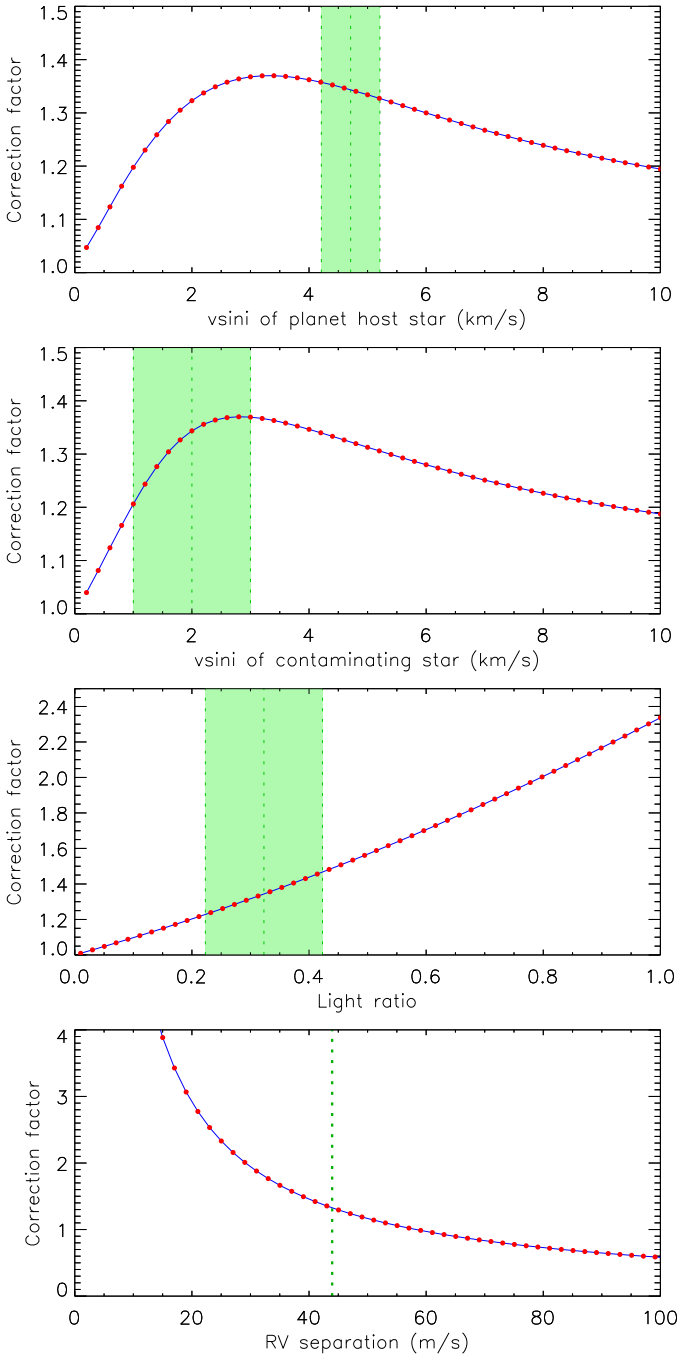

Fig. 2. Behaviour of the correction factor for WASP-20 in the case that the planet transits the brighter star. The correction factor is shown as a function of the $v \sin i$ values of the two stars, and of the light ratio. The bottom panel is included for reference and shows its variation as a function of the RV separation of the two stars. In each case the correction factor is shown using red points connected by blue lines, and the assumed system parameters are shown with their errorbars as green dotted lines, with the range of values allowed by the uncertainties indicated by light green shading.

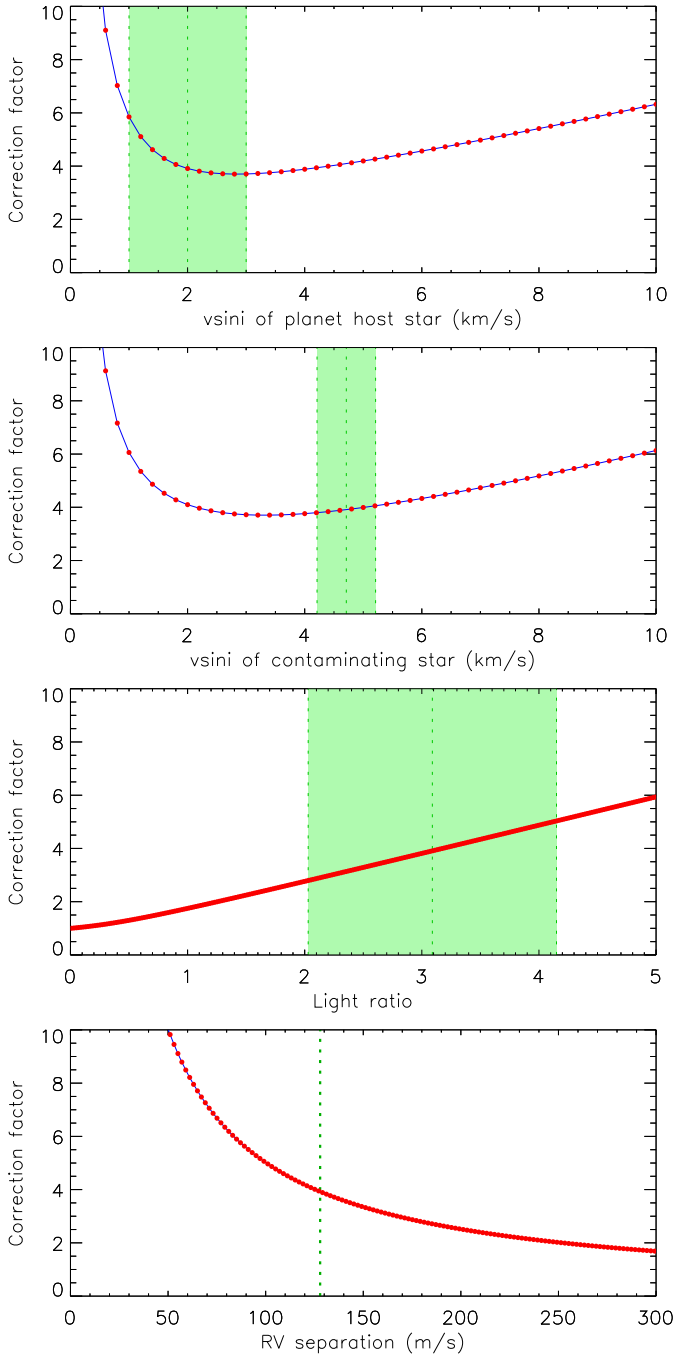

Fig. 3. Behaviour of the correction factor for WASP-20 in the case that the planet host star is the fainter star. Other comments are as for Fig. 2.

curves, thus the uncertainty in its measured contribution was ignored.

3.2.1. Photometric analysis

WASP-70 has not been observed using TESS due to its equatorial sky position, so we have analysed the system based on the best light curve we are aware of: the r-band *Euler*Cam data from the night of 2011 September 20 (Anderson et al. 2014). We determined an r-band light ratio of 0.073 ± 0.032 using the i-band magnitude difference of $\Delta i = 2.62 \pm 0.18$ from Wöllert & Brandner (2015) – this is preferable to our own ΔK value as it has the same precision and is much closer in wavelength.

The data were modelled and the system parameters were determined in the same way as for WASP-20. The results of this process are given in Table 3. We found that the limb darkening predicted by theoretical studies is too strong for this light curve, so we fitted for the linear coefficient in our final analyses.

Light curve fits for the scenario where the planet transits the fainter star are strongly disfavoured: the best fit we found had

Table 3. Derived physical properties for the WASP-70 system.

Parameter	Anderson et al. (2014)	This work (planet transits brighter star)
$r_A + r_b$		0.1312 ± 0.0083
k	0.0985 ± 0.0012	0.0976 ± 0.0020
i (°)	$87.12^{+1.24}_{-0.65}$	86.5 ± 0.9
r_A		0.1196 ± 0.0075
r_b		0.01166 ± 0.00086
M_A ($M_\odot$)	1.106 ± 0.042	1.111 ± 0.029 ± 0.017
R_A ($R_\odot$)	$1.215^{+0.064}_{-0.069}$	1.251 ± 0.079 ± 0.006
$\log g_A$ (cgs)	$4.314^{+0.052}_{-0.036}$	4.290 ± 0.055 ± 0.002
ρ_A ($\rho_\odot$)	$0.619^{+0.136}_{-0.077}$	0.57 ± 0.11
τ (Gyr)		$4.4\ ^{+0.7\ +1.2}_{-1.3\ -1.6}$
M_b (M_{Jup})	0.590 ± 0.022	0.592 ± 0.019 ± 0.006
R_b (R_{Jup})	$1.164^{+0.073}_{-0.102}$	1.186 ± 0.088 ± 0.006
g_b (m s^{-2})	$10.0^{+1.4}_{-1.1}$	10.4 ± 1.6
ρ_b (ρ_{Jup})	$0.375^{+0.104}_{-0.060}$	0.332 ± 0.076 ± 0.002
T_{eq} (K)	1376 ± 40	1433 ± 46
a (au)	0.04853 ± 0.00062	0.0486 ± 0.0004 ± 0.0003

Notes. Where two sets of errorbars are given, the first is the statistical uncertainty and the second is the systematic uncertainty.

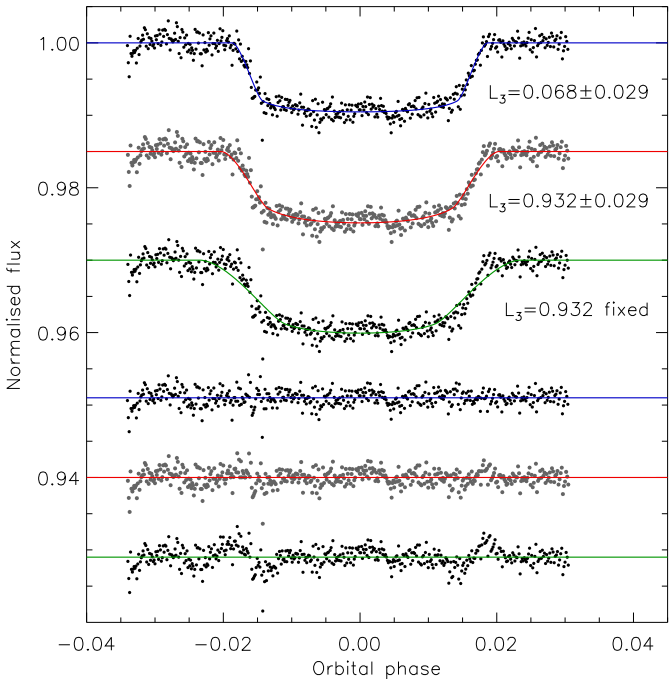

Fig. 4. Fit to the *Euler* telescope light curve of WASP-70. The observational data are shown as black and grey points. The JKTEBOP fits are shown for three scenarios: planet transiting brighter star; planet transiting fainter star; and planet transiting fainter star with the third light value forced to match that found from our direct image. The residuals of the fits are shown at the base of the figure with arbitrary offsets from zero.

χ^2 = 540, versus χ^2 = 467 under the assumption that the planet transits the brighter star. Both χ^2 values are for 467 datapoints and six fitted parameters, after the errorbars of the datapoints had been rescaled to give a reduced χ^2 of 1.0 for the best fits. We therefore rule out the possibility that the planet transits the fainter companion star. This supports our previous findings that third light is perfectly degenerate with other parameters of the fit (Southworth 2011) except in cases where it is at least 90% of the total light of the system (Bognár et al. 2015).

3.2.2. Physical properties

The angular separation of the planet host star and the contaminant, 3.2″, is significantly larger than the diameter of the optical fibres used to feed the CORALIE and HARPS spectrographs (2.0″ and 1.0″, respectively). We have therefore assumed that the brighter star is the planet host, and that there is no need to correct the RVs of the system for the presence of the fainter star.

Sousa et al. (2018) recently presented new atmospheric parameters for the host star: T_{eff} = 5864 ± 25 K and [Fe/H] = 0.21 ± 0.02. As in Sect. 3.1.3 we have adopted larger errorbars of 50 K and 0.05 dex for these quantities, respectively. Our results are given in Table 3 and are in good agreement with those of Anderson et al. (2014). This is unsurprising, as Anderson et al. (2014) accounted for the presence of the companion in their work. It is also encouraging, because Anderson et al. (2014) did not account for the uncertainty in the light contributed by the companion and thus potentially neglected an important source of uncertainty. We do find the star to be slightly larger: this causes an increase in the measured radius and equilibrium temperature of the planet, and a decrease in its measured density.

3.3. WASP-8

WASP-8 has the third-brightest nearby companion, with ΔK = 2.29 ± 0.08 mag and a separation of 4.52″. The companion was detected in the discovery paper of the system (Queloz et al. 2010), who did not comment on how (or whether) its presence was accounted for in their analysis. It was also detected in a subsequent adaptive-optics study (Ngo et al. 2015) and a Lucky-Imaging study (Evans et al. 2016b), and is visible in 2MASS images (Queloz et al. 2010). The *Gaia* DR2 database (Gaia Collaboration 2018) lists parallaxes and proper motions of the two objects that are consistent with each other, supporting their companionship.

3.3.1. Photometric analysis

WASP-8 has been observed using TESS and this light curve was treated in the same way as the one for WASP-20 (Sect. 3.1). Our ΔK value corresponds to a light ratio between the two stars of 0.0356 ± 0.0067 and thus a third light of L_3 = 0.0344 ± 0.0065. This was used to model the TESS light curve under the two alternative possibilities of which is the host star. WASP-8 has an eccentric orbit so we constrained the Poincaré elements to be $e \cos\omega$ = 0.02307 ± 0.00010 and $e \sin\omega$ = −0.0392 ± 0.0029 (Queloz et al. 2010).

As with WASP-70, we find that light curve fits for the scenario where the planet transits the fainter star are strongly disfavoured, with χ^2 = 1090 versus χ^2 = 674 for 668 degrees of freedom. These numbers again refer to the case where the errorbars of the TESS data, which are far too small, were rescaled to give a reduced χ^2 of approximately 1.0. There is also a large tension in the planet-transits-fainter-star scenario as the best-fitting

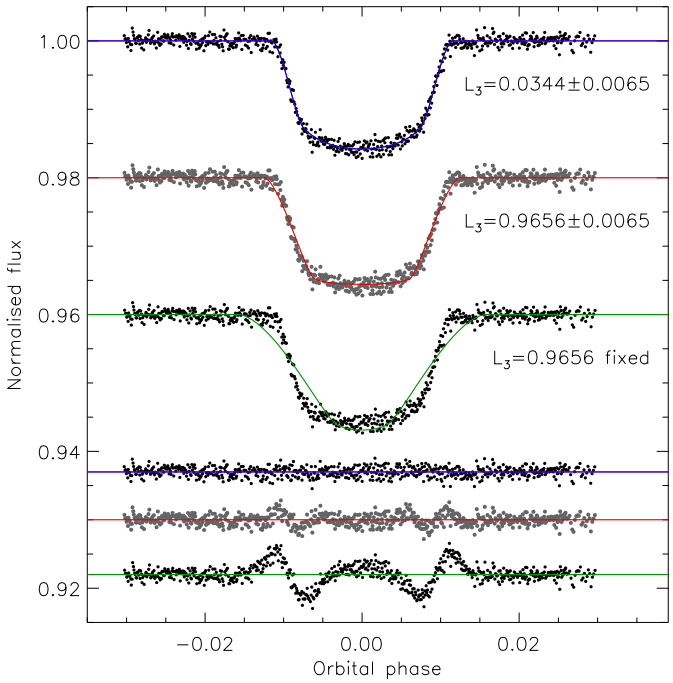

Fig. 5. Fits to the TESS light curve of WASP-8. The observational data are shown as black and grey points. The plotted quantities are otherwise the same as for Fig. 4.

value of third light disagrees with the applied prior at the 10σ level. The best fits for the two options (Fig. 5) clearly show a poor fit to the large-L_3 scenario. We therefore proceeded under the safe assumption that the planet transits the brighter star.

3.3.2. Physical properties

The angular separation of the planet host star and the contaminant is 4.5″ so, like WASP-70, is significantly larger than the entrance apertures of the spectrographs. We have therefore not corrected K_A for the presence of the nearby star. Mortier et al. (2013) gave the atmospheric parameters as $T_{\rm eff}$ = 5690 ± 36 K and [Fe/H] = 0.29 ± 0.03; we have adopted larger errorbars as in Sect. 3.1.3.

Our physical properties were calculated with these atmospheric parameters, the value of $K_A = 221.1 \pm 1.2\,{\rm m\,s^{-1}}$ given by Knutson et al. (2014), and the photometric parameters we determined from the TESS data above (Table 4). These give a significant improvement in the precision of the measured properties compared to those quoted by Queloz et al. (2010), primarily due to the availability of the TESS data. However, the high density of the star implies a rather young age and this puts it near the edge of the grids of theoretical stellar evolutionary models used in our study. This in turn causes a larger systematic error in the physical properties compared to the other stars in the current work. The young age is also in poor agreement with the lithium abundance determined by Queloz et al. (2010), a discrepancy which should be investigated in future using other age indicators such as kinematic properties and emission in the calcium H and K lines.

3.4. WASP-76

The companion of WASP-76 has a very similar magnitude difference to that of WASP-8, $\Delta K = 2.30 \pm 0.05$ mag, but a much smaller separation of 0.436″. The companion was not detected in the discovery paper of the system (West et al. 2016), but was found in a later work (Wöllert & Brandner 2015). It has been redetected in subsequent studies (Ginski et al. 2016; Ngo et al. 2016) and in Paper I we confirmed the common proper motion of the two objects.

In light of this it is worthwhile to reconsider the properties of WASP-76. However, it has not been observed using TESS and the available light curves (West et al. 2016) are either incomplete or riven with red noise. We therefore obtained a new transit light curve of WASP-76, and used this to refine the properties of the system. The light curve was observed on the night of 2017 October 26 using the CAHA 1.23 m telescope. The data were obtained with the telescope defocussed to increase the photometric precision (see Southworth et al. 2009), through a Cousins R filter, and using the standard approach of our group (e.g. Ciceri et al. 2015; Mancini et al. 2017). Data reduction was performed using the DEFOT pipeline (Southworth et al. 2009, 2014), yielding differential magnitudes relative to an optimal ensemble of comparison stars with timestamps on the BJD(TDB) timescale.

Table 4. Derived physical properties for the WASP-8 system.

Parameter	Queloz et al. (2010)	This work (planet transits brighter star)
$r_A + r_b$		0.0623 ± 0.0013
k	$0.1130^{+0.0015}_{-0.0013}$	0.1227 ± 0.0011
i (°)	$88.55^{+0.15}_{-0.17}$	88.51 ± 0.09
r_A	0.0549 ± 0.0024	0.0555 ± 0.0011
r_b	$0.00620^{+0.00036}_{-0.00033}$	0.00681 ± 0.00018
M_A ($M_\odot$)	$1.030^{+0.054}_{-0.061}$	1.093 ± 0.024 ± 0.023
R_A ($R_\odot$)	$0.945^{+0.051}_{-0.036}$	0.976 ± 0.020 ± 0.007
$\log g_A$ (cgs)	4.5 ± 0.1	4.498 ± 0.018 ± 0.003
ρ_A ($\rho_\odot$)	$1.22^{+0.17}_{-0.15}$	1.176 ± 0.070
τ (Gyr)	3–5	$0.3\,^{+0.9\ +0.1}_{-0.0\ -0.1}$
M_b ($M_{\rm Jup}$)	$2.244^{+0.079}_{-0.093}$	2.216 ± 0.035 ± 0.031
R_b ($R_{\rm Jup}$)	$1.038^{+0.007}_{-0.047}$	1.165 ± 0.032 ± 0.008
g_b (m s^{-2})		42.5 ± 2.3
ρ_b ($\rho_{\rm Jup}$)		1.31 ± 0.10 ± 0.01
$T_{\rm eq}$ (K)		947 ± 12
a (au)	$0.0801^{+0.0014}_{-0.0016}$	0.0817 ± 0.0006 ± 0.0006

Notes. Where two sets of errorbars are given, the first is the statistical uncertainty and the second is the systematic uncertainty.

3.4.1. Photometric analysis

Our ΔK value corresponds to a light ratio between the two stars of 0.105 ± 0.012 and thus a third light of $L_3 = 0.095 \pm 0.011$. This was used to model our R-band light curve under the two alternative possibilities of which is the host star. As with WASP-8 (Sect. 3.3), the fits for the planet-transits-fainter-star scenario are heavily disfavoured and can be discounted (see Fig. 6).

As an additional result, the transit we observed appeared approximately 8.6 min earlier than predicted by the ephemeris

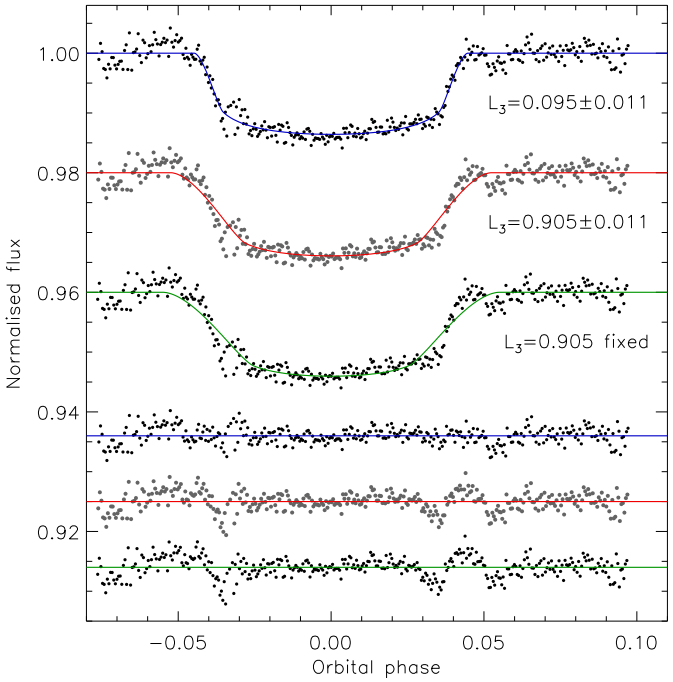

Fig. 6. Fit to the light curve of WASP-76 presented in the current work. The plotted quantities are otherwise the same as for Fig. 4.

from West et al. (2016). We therefore provide a revised orbital ephemeris for this system:

$$T_0 = \mathrm{BJD(TDB)}\,2\,458\,053.47655(34) + 1.8098798(5)E,$$

where E is the cycle number since the reference time and the bracketed quantities give the uncertainty in the last digit of the previous number. This ephemeris is based on our own transit and the reference time of mid-transit quoted by West et al. (2016). The orbital period is 0.54 s shorter than the one given in West et al. (2016), a change significantly larger than the errorbars. Further times of transit should be obtained in order to check if this system shows deviations from a constant orbital period. At present, the hypothesis that there are transit timing variations in the system is completely degenerate with the hypothesis that the errorbars for the original ephemeris are underestimated. The law of parsimony indicates we should assume the latter option at present.

3.4.2. Physical properties

The angular separation of the planet host star and the contaminant is 0.44″ so we operated under the assumption that the fainter star fully contaminated the spectrum and therefore the value of K_A must be corrected for this. We adopted $K_\mathrm{A} = 112 \pm 1\,\mathrm{m\,s^{-1}}$ and $v \sin i = 2.33 \pm 0.36\,\mathrm{km\,s^{-1}}$ from Brown et al. (2017) as the best estimates of these quantities, as they are based on a sophisticated modelling of the RVs and spectral line deformation during transit.

We found a correction factor of 1.111 with errorbars of ±0.006 from the $v \sin i$ of the brighter star, ±0.007 from the $v \sin i$ of the fainter star, and ±0.013 for the light ratio. Adding these uncertainties in quadrature gives a correction factor of 1.111 ± 0.016. This yields a velocity amplitude of $124.4 \pm 1.8\,\mathrm{m\,s^{-1}}$, where the uncertainties from the measurement and from the correction factor have again been added in quadrature. This change in K_A is modest but nevertheless significant at the 7σ level.

Table 5. Derived physical properties for the WASP-76 system.

Parameter	West et al. (2016)	This work (planet transits brighter star)
$r_\mathrm{A} + r_\mathrm{b}$		$0.276^{+0.014}_{-0.004}$
k	0.1090 ± 0.0007	$0.1126^{+0.0045}_{-0.0022}$
i (°)	$88.0^{+1.3}_{-1.6}$	$89.9^{+0.1}_{-4.3}$
r_A		$0.248^{+0.012}_{-0.004}$
r_b		$0.0280^{+0.0017}_{-0.0006}$
M_A ($M_\odot$)	1.46 ± 0.07	$1.356\,^{+0.048}_{-0.025}\,^{+0.009}_{-0.014}$
R_A ($R_\odot$)	1.73 ± 0.04	$1.716\,^{+0.086}_{-0.030}\,^{+0.004}_{-0.006}$
$\log g_\mathrm{A}$ (cgs)	4.128 ± 0.015	$4.101\,^{+0.015}_{-0.041}\,^{+0.001}_{-0.001}$
ρ_A ($\rho_\odot$)	$0.186^{+0.008}_{-0.018}$	$0.268^{+0.013}_{-0.035}$
τ (Gyr)		$1.0\,^{+0.3}_{-0.8}\,^{+0.2}_{-0.2}$
M_b (M_Jup)	0.92 ± 0.03	$0.914\,^{+0.025}_{-0.017}\,^{+0.004}_{-0.006}$
R_b (R_Jup)	$1.83^{+0.06}_{-0.04}$	$1.885\,^{+0.117}_{-0.042}\,^{+0.004}_{-0.006}$
g_b ($\mathrm{m\,s^{-2}}$)	6.31 ± 0.39	$6.38^{+0.30}_{-0.72}$
ρ_b (ρ_Jup)	0.151 ± 0.010	$0.1276\,^{+0.0088}_{-0.0208}\,^{+0.0004}_{-0.0003}$
T_eq (K)	2160 ± 40	2235^{+56}_{-25}
a (au)	0.0330 ± 0.0005	$0.03217\,^{+0.00038}_{-0.00020}\,^{+0.00007}_{-0.00011}$

Notes. Where two sets of errorbars are given, the first is the statistical uncertainty and the second is the systematic uncertainty.

Andreasen et al. (2017) gave atmospheric properties for the planet host star of $T_\mathrm{eff} = 6347 \pm 52$ K and [Fe/H] = 0.36 ± 0.04; we adopted a errorbar of 0.05 dex for [Fe/H] (see Sect. 3.1.3). With these properties, the corrected K_A, and the photometric parameters from our new light curve, we determined the physical properties of the system and give these in Table 5. The new light curve gives a lower density and thus lower mass for the star, which balances the corrected value of K_A so the measured planet mass is almost unchanged. However, the smaller semimajor axis and higher T_eff of the host star adopted in the current study yields a significantly hotter equilibrium temperature of the planet of 2235^{+56}_{-25} K.

WASP-76 b is one of the hottest planets known. As a result of this, its atmosphere has been the subject of several observational studies (Tsiaras et al. 2018; Seidel et al. 2019; Žák et al. 2019). These should be revisited now that the planetary system is known to have a close companion (Paper I) and the planet itself has a larger radius and higher measured equilibrium temperature (this work).

3.5. WASP-2

WASP-2 has a faint companion at an angular separation of 0.710″ that was discovered in the process of confirming the planetary nature of the system (Collier Cameron et al. 2007). The companion has been detected by several follow-up surveys (Daemgen et al. 2009; Bergfors et al. 2013; Ngo et al. 2015; Wöllert & Brandner 2015). Evans et al. (2016b) confirmed that the two objects have the same proper motion to 5σ significance, and tentatively identified orbital motion.

Table 6. Derived physical properties for the WASP-2 system.

Parameter	Value	Reference
$r_A + r_b$	0.1403 ± 0.0021	Southworth et al. (2010)
k	0.1326 ± 0.0007	Southworth et al. (2010)
i (°)	84.81 ± 0.17	Southworth et al. (2010)
r_A	0.1238 ± 0.0018	Southworth et al. (2010)
r_b	0.01643 ± 0.00030	Southworth et al. (2010)
M_A ($M_\odot$)	0.843 ± 0.033 ± 0.019	This work
R_A ($R_\odot$)	0.821 ± 0.013 ± 0.006	This work
log g_A (cgs)	4.536 ± 0.015 ± 0.003	This work
ρ_A ($\rho_\odot$)	1.524 ± 0.067	This work
τ (Gyr)	$7.6^{+2.5\ +3.2}_{-3.3\ -4.1}$	This work
M_b (M_{Jup})	0.892 ± 0.027 ± 0.013	This work
R_b (R_{Jup})	1.060 ± 0.024 ± 0.008	This work
g_b (m s^{-2})	19.70 ± 0.78	This work
ρ_b (ρ_{Jup})	0.701 ± 0.041 ± 0.005	This work
T_{eq} (K)	1286 ± 17	This work
a (au)	0.0308 ± 0.0004 ± 0.0002	This work

Notes. Where two sets of errorbars are given, the first is the statistical uncertainty and the second is the systematic uncertainty.

WASP-2 has not so far been observed using the TESS satellite, so the best transit light curves available are observations of three transits using the telescope-defocussing method by Southworth et al. (2010). These authors accounted for the presence of the nearby star in their analysis, with a magnitude difference very similar to that found in Paper I. There is no need to repeat this work, so we use their values of r_1, r_2 and i in our analysis.

However, the RVs of WASP-2 A have not been corrected for the effects of contamination from the nearby star, and this is why we have revisited the system here. The separation of the two stars is significantly smaller than that angular size of the optical fibre used to obtain the RVs by Collier Cameron et al. (2007), and comparable to the slit width for the observations presented by Knutson et al. (2014), which were obtained using the Keck telescope and HIRES spectrograph. We have assumed that the fainter star fully contaminates the spectrum of the planet host star in order to calculate the correction factor to K_A: if the contamination is smaller then the correction factor would be decreased approximately linearly so it would be easy to adjust these results in future.

To calculate the correction factor we adopted $v \sin i$ = 1.3 ± 0.5 km s^{-1} from the Rossiter-McLaughlin analysis of Albrecht et al. (2011), K_A = 156.7 ± 1.2 m s^{-1} from Knutson et al. (2014), and T_{eff} = 5170 ± 60 K from Southworth (2012). The light ratio of the system, determined as in Sect. 2.1, is 0.0204 ± 0.0039 for the Bessell R-band. The correction factor for these parameters is 1.014 with errorbars of ±0.006 from the $v \sin i$ of the brighter star, ±0.007 from the $v \sin i$ of the fainter star, and ±0.003 for the light ratio. Adding these uncertainties in quadrature gives a correction factor of 1.014 ± 0.010 and thus K_A = 158.9 ± 2.3 m s^{-1}.

Our measurements of the physical properties of the WASP-2 system are given in Table 6. They were calculated from the parameters given in the previous section, plus [Fe/H] = 0.04 ± 0.05 from Southworth (2012). We find results in good agreement with previous studies, the main difference being a slight increase in the measured mass of the planet and thus density and surface gravity.

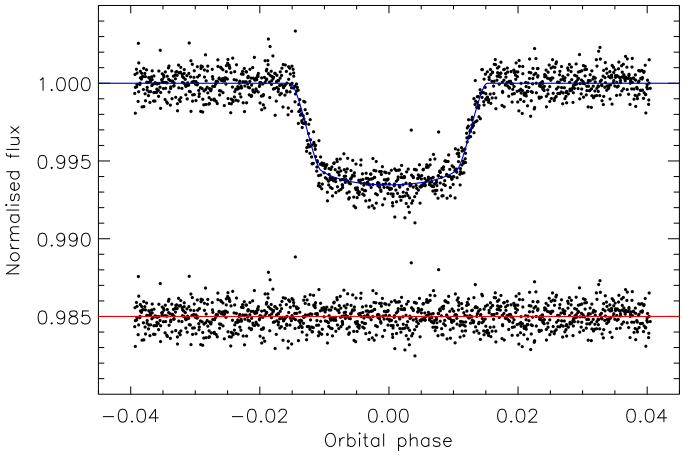

Fig. 7. Fit to the TESS light curve of WASP-131. Only the fit with the planet orbiting star A is shown.

3.6. WASP-131

The final system we have looked at in the current work is WASP-131. The companion star is relatively faint ΔK = 2.82 ± 0.20 but is very close (0.189″) and thus was previously unknown. There is also a TESS light curve for this object that was not available to past analyses. The planetary nature of WASP-131 was discovered by Hellier et al. (2017) and the system is of interest because the planet has a very low density and surface gravity.

3.6.1. Photometric analysis

We obtained the TESS light curve and extracted the transits in the same way as in Sect. 3.1. Our ΔK value corresponds to a light ratio between the two stars of 0.025 ± 0.012 and thus a third light of L_3 = 0.024 ± 0.012. This was used to model the TESS light curve for the scenario where the planet orbits the brighter star (Fig. 7). We did not consider the planet-orbits-fainter star scenario because the analyses of WASP-8 and WASP-76 above make it clear that this possibility is not able to provide a good fit to the transit light curve when $\Delta K \gtrapprox 2.3$ mag.

3.6.2. Physical properties

We obtained a correction factor for K_A under the assumption that all light from the fainter star contaminated the spectrum, and the measured K_A and $v \sin i$ are 30.5 ± 1.7 m s^{-1} and 3.0 ± 0.9 km s^{-1}, respectively (Hellier et al. 2017). We found a correction factor of 1.0269 with errorbars of ±0.0001 from the $v \sin i$ of the brighter star, ±0.0003 from the $v \sin i$ of the fainter star, and ±0.0014 for the light ratio. The final uncertainty dominates all others so we adopted it as the errorbar for the correction factor. This yields a velocity amplitude of 31.3 ± 1.8 m s^{-1}. This change in K_A is titchy and indicates that the contaminating light is sufficiently small that it does not have a significant effect on the RVs.

We used the stellar atmospheric properties of T_{eff} = 5950 ± 100 K and [Fe/H] = −0.18 ± 0.08 from Hellier et al. (2017), and our new values of r_1, r_2 and i from the TESS light curve, to determine the physical properties of the system. Our results are shown

Table 7. Derived physical properties for the WASP-131 system.

Parameter	Hellier et al. (2017)	This work (planet transits brighter star)
$r_A + r_b$		0.1284 ± 0.0049
k	0.0815 ± 0.0007	0.08112 ± 0.00083
i (°)	i = 85.0 ± 0.3	85.03 ± 0.37
r_A		0.1188 ± 0.0045
r_b		0.00964 ± 0.00042
M_A ($M_\odot$)	1.06 ± 0.06	1.002 ± 0.046 ± 0.025
R_A ($R_\odot$)	1.53 ± 0.05	1.526 ± 0.064 ± 0.013
log g_A (cgs)	4.089 ± 0.026	4.072 ± 0.033 ± 0.004
ρ_A ($\rho_\odot$)	0.292 ± 0.026	0.282 ± 0.032
τ (Gyr)	4.5 to 10	$7.2^{+0.8\ +0.9}_{-1.6\ -1.0}$
M_b (M_{Jup})	0.27 ± 0.02	0.270 ± 0.018 ± 0.004
R_b (R_{Jup})	1.22 ± 0.05	1.204 ± 0.056 ± 0.010
g_b (m s^{-2})	4.17 ± 0.38	4.62 ± 0.48
ρ_b (ρ_{Jup})	0.15 ± 0.02	0.145 ± 0.021 ± 0.001
T_{eq} (K)	1460 ± 30	1450 ± 36
a (au)	0.0607 ± 0.0009	0.0597 ± 0.0009 ± 0.0005

Notes. Where two sets of errorbars are given, the first is the statistical uncertainty and the second is the systematic uncertainty.

in Table 7 and are in excellent agreement with those from Hellier et al. (2017). In particular, the uncertainties in most parameters are very similar between the two studies despite the availability of the TESS light curve, suggesting those in the previous study were underestimated.

4. Population studies of transiting planetary systems

The measured masses, radii and densities of the bulk population of transiting planets can be used to study their internal structure or formation mechanisms. It is important to correct for the effects of stellar multiplicity in such work, in order to decrease biases that might affect the results. Our SPHERE survey, coupled with the results presented in the current work, allowed us to investigate the size of these corrections.

Ciardi et al. (2015) used stellar multiplicity rates for systems with separations of 1″ or less to infer that the mean planet radius correction factor, $\langle X_R \rangle$, is 1.5 for the *Kepler* Objects of Interest (KOIs: planet candidates discovered using the *Kepler* satellite). This quantity is given in the sense that one should multiply the measured radii of a population of planet candidates by $\langle X_R \rangle$ before comparing them to theoretical predictions of their physical properties. Ciardi et al. (2015) further broke this down into $\langle X_R \rangle \sim 1.6$ for hotter planet host stars (A-, F- and G-type) and $\langle X_R \rangle \sim 1.2$ for cooler ones (types K and M). They also noted that detailed follow-up observations including high-resolution imaging would bring $\langle X_R \rangle$ down from about 1.6 to 1.2, that brighter systems such as those discovered by K2 and TESS would have $\langle X_R \rangle \sim 1.1$, and that the planet density would be more strongly affected because $\rho_b \propto R_b^{\ 3}$.

Furlan et al. (2017) discussed 1903 KOIs observed using new and published high-resolution images obtained with a variety of techniques, finding a total of 2297 nearby objects. They found that $\langle X_R \rangle$ was 1.09 or 3.09, under the assumption that the planets orbit the brighter or fainter stars, respectively. They expected the true value to be closer to the lower end of the range defined by these two values, and suggested $\langle X_R \rangle$ = 1.5–2.0. Hirsch et al. (2017) concentrated on the stars within this sample hosting small planets ($R_2 < 5\,R_\oplus$) and having companions within 2″, and found $\langle X_R \rangle$ = 1.65 under the assumption that each planet was equally likely to orbit either of the two stars.

Ziegler et al. (2020) presented a study of 542 TESS transiting planet candidates using speckle imaging. They found $\langle X_R \rangle$ = 1.11 if the planets orbited the brighter stars and $\langle X_R \rangle$ = 2.55 if they orbited the fainter stars, with an average of $\langle X_R \rangle$ = 1.82 if the planets were equally likely to orbit either star. A similar study of the KOIs by Ziegler et al. (2018) returned a value of $\langle X_R \rangle$ = 1.54 for the last situation.

With our survey of 45 transiting planetary systems (Paper I) and corrections to the measured physical properties (this work) we were in a position to calculate $\langle X_R \rangle$ for a sample of planetary systems. We restricted our analysis to hot Jupiters, which we defined in this case as planets of mass >0.2 M_{Jup} and orbital period <12 d. These restrictions removed four of the planets studied in Paper I (K2-24, K2-38, K2-39 and K2-99), leaving us with a sample of 41 objects.

We first calculated X_R for each of the six systems studied in this work, from the physical properties we measured with and without accounting for contamination. For WASP-20, where it is not yet clear which star hosts the planet, we calculated X_R for both scenarios and took the average. For the remaining systems, where our light curve fits discount the possibility that the planet orbits the fainter star, we calculated X_R under the assumption that the planet orbits the brighter star in each case. For the remaining 35 systems we adopted X_R = 1.0 as there are no detected companions bright enough to make a significant difference to the measured physical properties (see Sect. 3.6). This means that our $\langle X_R \rangle$ is suitable for application to the bulk population of hot Jupiters.

We find a mean planet radius correction factor of $\langle X_R \rangle$ = 1.009 ± 0.045 (standard deviation σ = 0.016). The uncertainty has been propagated from the individual values for each X_R, and does not account for the small sample size. This is much smaller than found in previous works (see above). The first reason for this is that we included all observed systems rather than just those with a known companion, thus making our results more widely applicable to populations of planetary systems. The second reason is that large values of X_R are obtained when a planet orbits the fainter of two stars, but we were able to rule out this possibility in all cases but one. Most previous works have assumed an equal probability for which star hosts the planet, which ignores situations when the data are only consistent with one scenario, and also neglects changes in planet occurrence rates as a function of host star mass.

We were also in a position to calculate corrections to planet mass. Using the same procedure as above, and accounting for the fact that some planet masses are unchanged because the light from the nearby star fell outside the entrance aperture of the spectrograph, we find $\langle X_M \rangle$ = 1.031 ± 0.019 (σ = 0.019). This is once again a small correction, but is driven to a larger value than $\langle X_R \rangle$ because of the large effect of contaminating light in the case of WASP-20 b (Table 2).

Finally, we have calculated the mean planet density correction factor to be $\langle X_\rho \rangle$ = 0.995 ± 0.046 (σ = 0.078). This result is counter to the expectation that $\langle X_\rho \rangle$ would be significantly larger than $\langle X_R \rangle$, and this occurs for two reasons. First, contaminating light causes both the measured planet mass and radius to decrease, and partial cancellation of these effects yields

values of X_ρ that are not much larger than unity (i.e. contamination causes the measured density to decrease). Second, in some cases (e.g. WASP-70 and WASP-8), the source of contaminating light is several arseconds from the planetary system. In such cases it affects the light curve but not the RVs, resulting in values of X_ρ that are below unity (i.e. contamination causes the measured density to increase). The net result is that $\langle X_\rho \rangle$ is approximately unity for the sample considered here, but with a large scatter.

We have therefore obtained mean correction factors that can be applied to the masses, radii, and densities of transiting hot Jupiter systems. Our sample selection (Paper I) was based only on target brightness and observability: it was agnostic about the physical properties of the planetary systems or whether a nearby companion was already known. Our sample is therefore representative of bright hot Jupiters predominantly discovered using ground-based surveys. The mean correction factors we have derived are suitable for application to similar samples of transiting planets, but not to samples with significantly different properties. In particular, the mean correction factors are likely to be larger for smaller planets because their shallower transits can be adequately fitted with a wider range of contamination levels, smaller for more nearby planetary systems because a larger fraction of bound companions will be resolved, and more scattered for planetary systems in crowded areas of the sky due to the wider variety of systemic velocities of contaminating objects.

5. Summary and conclusions

We have presented a detailed analysis of six transiting planetary systems in order to account for the effect of fainter nearby stars on the measured physical properties of the system. For one of these systems the nearby star was discovered in Paper I, and for the remaining five it was detected in previous studies. Contaminating light affects the photometric properties of a system: it dilutes the transit depth and biases the measured planet radius to lower values. It also affects spectroscopic analysis by contaminating the CCFs from which RVs are measured, causing a decrease in the RV variation and thus an underestimate of the planet mass. We used an existing approach to ameliorate the photometric bias and presented a new method to account for the RV bias.

WASP-20 is the system most affected because its nearby star is relatively bright. Our analysis of this system agrees well with that of Evans et al. (2016a) and is an improvement because of the availability of a high-quality light curve from the TESS satellite. The second system, WASP-70, has a contaminant that is sufficiently distant to leave the spectroscopy of this system unaffected, and sufficiently faint to have only a small effect on the photometric properties of the planetary system. A similar story occurs for WASP-8, although a significant improvement in its characterisation is achieved using the TESS light curve. The final three systems, WASP-76, WASP-2 and WASP-131, all have contaminating stars within 0.7″ that are nevertheless sufficiently faint to make little difference to measurements of their physical properties. The updated physical properties of the systems have been lodged in the TEPCat catalogue[5] (Southworth 2011).

Looking at Paper I, we see no other systems that would significantly benefit from the analysis of individual objects as presented above. Our results for WASP-131 showed that a contaminating star fainter by $\Delta K = 2.80$ mag is too faint to make much difference to the measured physical properties of planetary systems such as those studied in the current work. Only one more object in Paper I has a ΔK smaller than this: HAT-P-41 has $\Delta K = 2.50 \pm 0.21$ mag; and this star was already known and accounted for (Hartman et al. 2012). We have used our sample of 45 transiting hot Jupiter systems, and the corrections to their measured properties needed to account for contaminating light, to determine mean correction factors for samples of planet masses, radii, and densities. We find $\langle X_{\rm M} \rangle = 1.031 \pm 0.019$, $\langle X_{\rm R} \rangle = 1.009 \pm 0.045$ and $\langle X_\rho \rangle = 0.995 \pm 0.046$, respectively. The radius correction is much smaller than found by other studies, primarily because we were able to reject the possibility that the planet orbits the fainter star for five out of the six systems we studied in detail. The mass and density corrections are also small, and to our knowledge are the first ones to be published. The mean correction factors will depend on the population of objects under consideration, specifically on the planet radius, system distance, and sky position (via the amount of field star contamination).

We conclude that it is important to obtain high-resolution observations of transiting planetary systems in order to detect cases like WASP-20 and Kepler-14, where the physical properties are strongly affected by the presence of a nearby star, but that these cases are sufficiently rare that they will have a negligible influence on studies of the overall population of planetary systems. This is good news.

Acknowledgements. The research of A.J.B. leading to these results has received funding from the European Research Council under ERC Starting Grant agreement 678194 (FALCONER). The following internet-based resources were used in research for this paper: the ESO Digitized Sky Survey; the NASA Astrophysics Data System; the SIMBAD database operated at CDS, Strasbourg, France; and the arχiv scientific paper preprint service operated by Cornell University.

References

Albrecht, S., Winn, J. N., Johnson, J. A., et al. 2011, ApJ, 738, 50
Anderson, D. R., Collier Cameron, A., Delrez, L., et al. 2014, MNRAS, 445, 1114
Anderson, D. R., Collier Cameron, A., Hellier, C., et al. 2015, A&A, 575, A61
Andreasen, D. T., Sousa, S. G., Tsantaki, M., et al. 2017, A&A, 600, A69
Bakos, G. Á., Lázár, J., Papp, I., Sári, P., & Green, E. M. 2002, PASP, 114, 974
Baranne, A., Queloz, D., Mayor, M., et al. 1996, A&AS, 119, 373
Baruteau, C., Crida, A., Paardekooper, S.-J., et al. 2014, Protostars and Planets VI (Tucson: University of Arizona Press), 667
Bergfors, C., Brandner, W., Daemgen, S., et al. 2013, MNRAS, 428, 182
Beuzit, J. L., Vigan, A., Mouillet, D., et al. 2019, A&A, 631, A155
Bognár, Z., Lampens, P., Frémat, Y., et al. 2015, A&A, 581, A77
Bohn, A. J., Southworth, J., Ginski, C., et al. 2020, A&A, 635, A73
Borucki, W. J., Koch, D., Basri, G., et al. 2010, Science, 327, 977
Boss, A. P. 1995, Science, 267, 360
Brown, T. M. 2001, ApJ, 553, 1006
Brown, D. J. A., Triaud, A. H. M. J., Doyle, A. P., et al. 2017, MNRAS, 464, 810
Buchhave, L. A., Latham, D. W., Carter, J. A., et al. 2011, ApJS, 197, 3
Chatterjee, S., Ford, E. B., Matsumura, S., & Rasio, F. A. 2008, ApJ, 686, 580
Ciardi, D. R., Beichman, C. A., Horch, E. P., & Howell, S. B. 2015, ApJ, 805, 16
Ciceri, S., Mancini, L., Southworth, J., et al. 2015, A&A, 577, A54
Collier Cameron, A., Bouchy, F., Hébrard, G., et al. 2007, MNRAS, 375, 951
Daemgen, S., Hormuth, F., Brandner, W., et al. 2009, A&A, 498, 567
Davies, M. B., Adams, F. C., Armitage, P., et al. 2014, in Protostars and Planets VI, eds. H. Beuther, R. S. Klessen, C. P. Dullemond, & T. Henning (Tucson: University of Arizona Press), 787
De Pascale, M., Worley, C. C., de Laverny, P., et al. 2014, A&A, 570, A68
Evans, D. F., Southworth, J., & Smalley, B. 2016a, ApJ, 833, L19
Evans, D. F., Southworth, J., Maxted, P. F. L., et al. 2016b, A&A, 589, A58
Evans, D. F., Southworth, J., Smalley, B., et al. 2018, A&A, 610, A20
Fabrycky, D., & Tremaine, S. 2007, ApJ, 669, 1298

[5] http://www.astro.keele.ac.uk/jkt/tepcat/

Fragner, M. M., Nelson, R. P., & Kley, W. 2011, A&A, 528, A40
Furlan, E., Ciardi, D. R., Everett, M. E., et al. 2017, AJ, 153, 71
Gaia Collaboration (Brown, A. G. A., et al.) 2018, A&A, 616, A1
Ginski, C., Mugrauer, M., Seeliger, M., et al. 2016, MNRAS, 457, 2173
Gómez Maqueo Chew, Y., Morales, J. C., Faedi, F., et al. 2014, A&A, 572, A50
Hartman, J. D., Bakos, G. Á., Béky, B., et al. 2012, AJ, 144, 139
Hellier, C., Anderson, D. R., Cameron, A. C., et al. 2017, MNRAS, 465, 3693
Hirsch, L. A., Ciardi, D. R., Howard, A. W., et al. 2017, AJ, 153, 117
Jofré, P., Heiter, U., Soubiran, C., et al. 2014, A&A, 564, A133
Knutson, H. A., Fulton, B. J., Montet, B. T., et al. 2014, ApJ, 785, 126
Kopal, Z. 1959, Close Binary Systems, The International Astrophysics Series (Hoboken: Wiley)
Kraus, A. L., Ireland, M. J., Huber, D., Mann, A. W., & Dupuy, T. J. 2016, AJ, 152, 8
Lin, D. N. C., Bodenheimer, P., & Richardson, D. C. 1996, Nature, 380, 606
Mancini, L., Southworth, J., Raia, G., et al. 2017, MNRAS, 465, 843
Marcy, G. W., & Butler, R. P. 1996, ApJ, 464, L147
Mayor, M., & Queloz, D. 1995, Nature, 378, 355
Moe, M., & Kratter, K. M. 2019, MNRAS, submitted, [arXiv:1912.01699]
Mortier, A., Santos, N. C., Sousa, S. G., et al. 2013, A&A, 558, A106
Naoz, S., Farr, W. M., Lithwick, Y., Rasio, F. A., & Teyssandier, J. 2011, Nature, 473, 187
Ngo, H., Knutson, H. A., Hinkley, S., et al. 2015, ApJ, 800, 138
Ngo, H., Knutson, H. A., Hinkley, S., et al. 2016, ApJ, 827, 8
Pollacco, D. L., Skillen, I., Cameron, A. C., et al. 2006, PASP, 118, 1407
Queloz, D., Anderson, D., Collier Cameron, A., et al. 2010, A&A, 517, L1
Rasio, F. A., & Ford, E. B. 1996, Science, 274, 954
Ricker, G. R., Winn, J. N., Vanderspek, R., et al. 2015, J. Astron. Telesc. Instrum. Syst., 1, 014003
Roell, T., Neuhäuser, R., Seifahrt, A., & Mugrauer, M. 2012, A&A, 542, A92
Ryabchikova, T., Piskunov, N., Pakhomov, Y., et al. 2016, MNRAS, 456, 1221
Seager, S., & Sasselov, D. D. 2000, ApJ, 537, 916
Seidel, J. V., Ehrenreich, D., Wyttenbach, A., et al. 2019, A&A, 623, A166
Sousa, S. G., Adibekyan, V., Delgado-Mena, E., et al. 2018, A&A, 620, A58
Southworth, J. 2008, MNRAS, 386, 1644
Southworth, J. 2009, MNRAS, 394, 272
Southworth, J. 2010, MNRAS, 408, 1689
Southworth, J. 2011, MNRAS, 417, 2166
Southworth, J. 2012, MNRAS, 426, 1291
Southworth, J. 2013, A&A, 557, A119
Southworth, J., & Evans, D. F. 2016, MNRAS, 463, 37
Southworth, J., Hinse, T. C., Jørgensen, U. G., et al. 2009, MNRAS, 396, 1023
Southworth, J., Mancini, L., Calchi Novati, S., et al. 2010, MNRAS, 408, 1680
Southworth, J., Hinse, T. C., Burgdorf, M., et al. 2014, MNRAS, 444, 776
Southworth, J., Mancini, L., Ciceri, S., et al. 2015, MNRAS, 447, 711
Tsiaras, A., Waldmann, I. P., Zingales, T., et al. 2018, AJ, 155, 156
Udry, S., & Santos, N. C. 2007, ARA&A, 45, 397
Wang, J., Fischer, D. A., Horch, E. P., & Xie, J.-W. 2015, ApJ, 806, 248
West, R. G., Hellier, C., Almenara, J.-M., et al. 2016, A&A, 585, A126
Wöllert, M., & Brandner, W. 2015, A&A, 579, A129
Wu, Y., & Murray, N. 2003, ApJ, 589, 605
Žák, J., Kabáth, P., Boffin, H. M. J., Ivanov, V. D., & Skarka, M. 2019, AJ, 158, 120
Ziegler, C., Law, N. M., Baranec, C., et al. 2018, AJ, 155, 161
Ziegler, C., Tokovinin, A., Briceno, C., et al. 2020, AJ, 159, 19